Optics Communications 300 (2013) 244–248

Contents lists available at SciVerse ScienceDirect

Optics Communications

journal homepage: www.elsevier.com/locate/optcom

Functional facets for nonlinear crystals

Asia Shapira [a,*], Ana Libster [a], Yigal Lilach [b], Ady Arie [a]

[a] Department of Physical Electronics, School of Electrical Engineering, Tel Aviv University, Tel Aviv 69978, Israel
[b] Tel Aviv University Center for Nanoscience and Nanotechnology, Tel Aviv 69978, Israel

ARTICLE INFO

Article history:
Received 6 December 2012
Received in revised form
29 January 2013
Accepted 4 March 2013
Available online 28 March 2013

Keywords:
Second harmonic generation
Beam shaping
Focused ion beam
Computer generated hologram

ABSTRACT

We report on a new optical device allowing to efficiently add desired functionalities to a nonlinear interaction. This is achieved by focused ion beam patterning of a nano-layer of gold sputtered at the exit facet of a nonlinear crystal. The functionality is experimentally demonstrated with three examples: spatial filtering where a fundamental beam with a poor mode quality and its' frequency-doubled beam are filtered thereby providing high mode quality beams, focusing of a generated second harmonic beam and beam shaping where a fundamental Gaussian beam is transformed into any arbitrary desired frequency-doubled beam. For the latter two examples, the functional facet also provides angular separation of the fundamental and second harmonic beams.

1. Introduction

In a typical nonlinear interaction, a Gaussian pump beam is sent into a nonlinear device, and generates another Gaussian beam at a new wavelength, which is then routed, filtered or shaped by various elements—mirrors, lenses, pinholes, gratings, spatial light modulators, etc. In order to save space and cost, it is desired to combine the nonlinear process and the above mentioned functions into a single element. The main approach to achieve this was based so far on spatial modulation of the second order nonlinear coefficient, which enables to quasi phase-match the nonlinear interaction, and at the same time to focus [1,2], steer [3], or shape [4–7] the nonlinearly generated beam. However, this approach has several limitations, for example, it is difficult to efficiently phase-match the interactions and shape the generated beam in the two transverse dimensions [6]. Moreover, it is difficult to apply complex modulation patterns to some of the more efficient crystals, e.g. $KTiOPO_4$. In this letter we suggest, for the first time to our knowledge, a new method for functionalizing a nonlinear process in a single crystal. This is achieved by a combination of a standard quasi phase-matched process in the crystal, followed by spatially patterning a nano-layer of gold sputtered on the exit facet of the crystal for achieving the desired functionality. The patterning is performed here by focused ion-beam (FIB) milling.

Functionality can be for example two-dimensional shaping of the generated beam, which can be achieved by binary patterning the gold according to a design of a computer generated hologram (CGH) [8]. Both the pump beam and the generated beam are transmitted through the hologram and a desired beam shape is formed at far field, at the first diffraction order. Since the central angle of the diffraction order is proportional to the wavelength, this method also separates the beams. Another example of functionality is beam quality improvement, which can be achieved by spatially filtering the beams, using a pattern of a pinhole.

2. Experiments and results

To demonstrate the concept of adding a functional facet to nonlinear crystals we fabricated a crystal aimed to shape, focus or improve the quality of a generated second harmonic (SH) beam. Shaping was planned for two types of beams, accelerating beams, including both a two-dimensional airy beam [9] and two orders ($n=2,4$) of Parabolic beams [10] and Laguerre–Gauss vortex beams [11] with topological charge $+1$ and $+2$. This variety is proposed to demonstrate the flexibility of the suggested technique. The binary amplitude transmission function of the gold layer was designed according to Ref. [12],

$$t(y,z) = 0.5[1 + sign\ \{\cos(2\pi y f_{carrier} + \varphi(y,z)) - \cos(\pi q(y,z))\}] \quad (1)$$

where $q(y,z)$ is defined by $\sin[\pi^* q(y,z)] = A(y,z)$ [12]. $A(y,z)$ and $\varphi(y,z)$ are the amplitude and the phase, respectively, of the Fourier transform (FT) of the desired wave-front in the first diffraction order. $A(y,z)$ is normalized to the range 0–1 and $\varphi(y,z)$ is in the range $0–2\pi$, $f_{carrier}$ is the frequency of the carrier function. The layer serves as a binary transmission hologram, so that the desired shape is obtained at the holograms' first diffraction order. This technique was also

* Corresponding author. Tel.: +972 545 289040.
E-mail addresses: asiasapi@gmail.com, asiasapi@post.tau.ac.il (A. Shapira).

0030-4018/$ - see front matter © 2013 Elsevier B.V. All rights reserved.
http://dx.doi.org/10.1016/j.optcom.2013.03.007

employed to encode a quadratic phase in order to focus the generated beam at the first diffraction order.

A pinhole was fabricated to demonstrate beam quality improvement. The pattern in the gold in this case was a circular aperture,

$$t(y,z)=\begin{cases}1 & \sqrt{y^2+z^2}\le R,\\ 0 & otherwise,\end{cases} \tag{2}$$

where R is the radius of the pinhole. A schematic illustration of the experimental setup is presented in Fig. 1. A fundamental frequency (FF) beam is entering the nonlinear crystal propagating along its' X axis, the crystal is periodically poled in this direction to allow for an efficient generation of SH. The patterned nano-layer of gold is located at the exit facet of the crystal in the Y–Z plane. The figure shows a simulation result for the far field output at both FF and SH for shaping of a vortex beam with a topological charge of $+2$. The angle of diffraction is $\sim\lambda m f_{carrier}$, where λ is the diffracted wavelength and m is the diffraction order, hence, the first diffraction order of the SH is separated from the FF wave, whereas the second order of the SH is located at nearly the same angle as the first order of the FF.

We tested the functional facet concept using two crystals, which were both designed to quasi phase-match an e-polarized second harmonic generation of an e-polarized 1064.5 nm pump. The first crystal was a $16\times7\times0.7$ mm^3 ($X\times Y\times Z$) stoichiometric

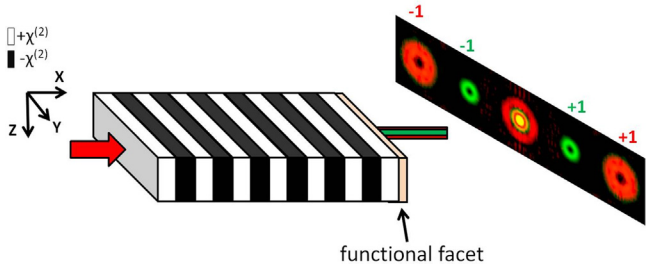

Fig. 1. Schematic illustration of the experimental setup, example of far field for a vortex beam with $l_c=+2$, showing the first diffraction orders of both frequencies.

lithium tantalate (SLT) crystal with a region of $16\times3\times0.7$ mm^3 being periodically poled with a period of 7.72 μm [13]. Electric field poling in ferroelectric crystals [14] is a process in which the direction of polarization along the Z axis of the crystal (and consequently the sign of the quadratic nonlinear coefficient) is set according to a chosen design, in our case a one-dimensional periodic structure. The second crystal was a $10\times2\times0.7$ mm^3 periodically poled $KTiOPO_4$ crystal with a period of 9 μm [15]. In both cases, a 80 nm of gold was sputtered on the 2×0.7 mm^2 or 7×0.7 mm^2 exit facets. Seven different structures of about 300×300 μm^2 and 600×600 μm^2 (for the lens structure) were then milled in the gold layer with FIB (Raith ionLINE). The carrier frequency, as defined in Eq. (1), in all structures was 6×10^4 m^{-1}, except for the parabolic structures where a value of 1.2×10^5 m^{-1} was used. The FIB used a 35 kV Gallium beam with a current of 1.7 nA. The time required for milling is determined by the size, resolution and the complexity of the desired pattern. In the case of a vortex beam with topological charge $+1$, for example, the milling time was 50 minutes. The process is calibrated by monitoring the secondary electron image from the sample, which is significantly changed when the gold layer is completely removed. Fig. 2, part (a) shows the method of mounting the nonlinear crystal, so that its' rather thin exit surface could be milled using the FIB. Parts (b)–(h) of the figure show microscopic pictures of the nano-patterned gold film structures, demonstrating the high quality and precision of the FIB milling process.

The FF source used in the optical experiment was a Nd:YAG laser producing 10 ns pulses at a 2 kHz repetition rate. For shaping experiments, the laser beam was focused at the center of the crystal creating a waist radius of approximately 100 μm. In focusing experiments the radius was set to approximately 300 μm. A beam with a 100 μm waist ensures an almost constant phase illuminating the encoded structures: For this beam a maximal deviation of 0.25 rad is expected in the SH beam upon impinging the holographic pattern at the exit facet. For the spatial filter experiments, a 100 μm beam was focused at the exit facet of the crystal, instead of the crystal center. This had a negligible effect on the nonlinear conversion efficiency, since the beams' Rayleigh range is three times larger than the crystal.

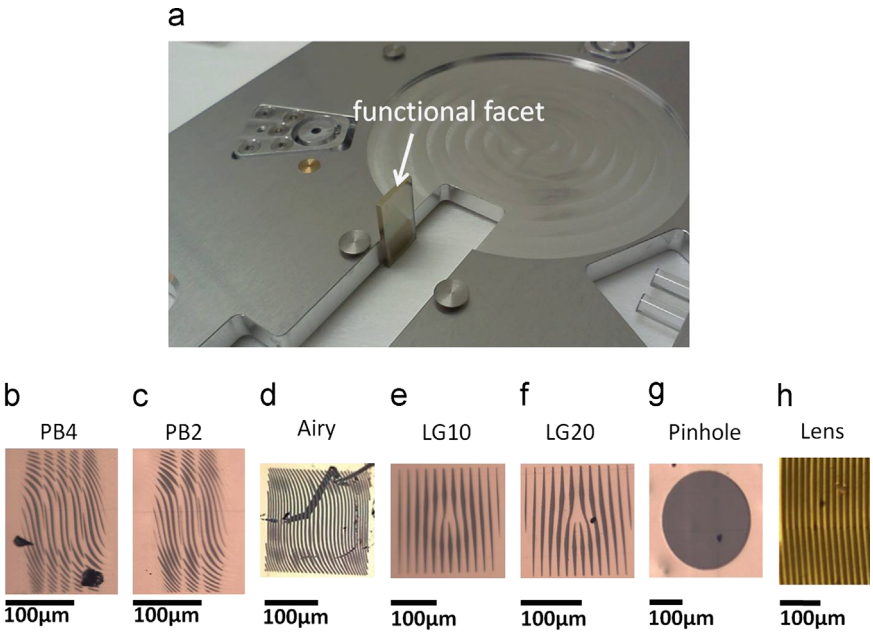

Fig. 2. Processing the crystals' facet in FIB. Placement of the SLT crystal before entering the FIB in order to pattern its rather thin exit facet (a) and microscopic pictures of the structures on the facet after the FIB milling (b)–(h).

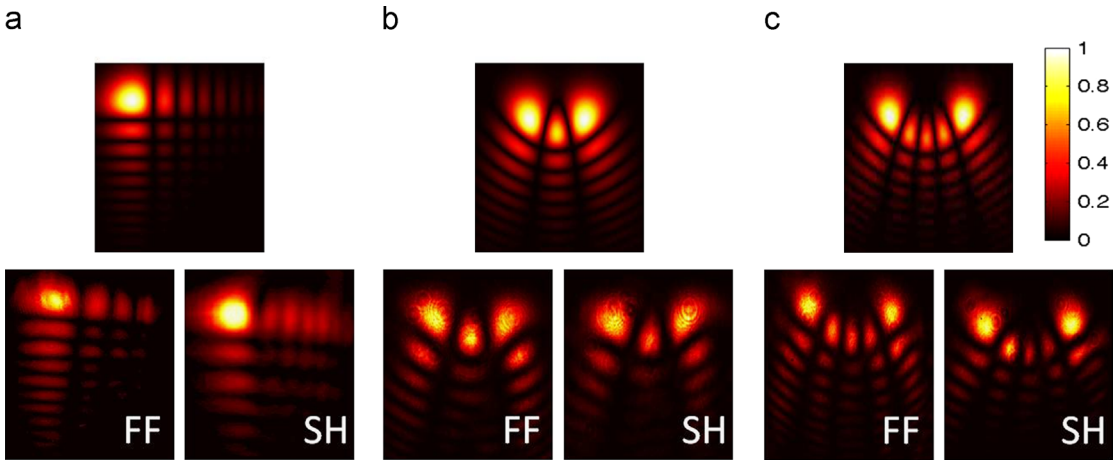

Fig. 3. Accelerating beams-theoretical beam (top row), FF generated beam and SH generated beam (bottom row). Airy beam (a), parabolic beams with $n=2$ (b), and $n=4$ (c).

Table 1
Comparison between predicted and measured diffraction parameters for FF and SH and measured beam profile spatial correlation.

	Prediction		Measurement			
	FF 1st order [%]	SH 1st order [%]	FF 1st order [%]	SH 1st order [%]	FF spatial corr.	SH spatial corr.
Airy	23.1	24.2	8.7	15.2	0.94	0.94
PB2	30.3	22.4	14.2	13.1	0.91	0.93
PB4	30.2	22.6	14.7	10.7	0.9	0.93
LG10	22	21.6	16	13.5	0.96	0.92
LG20	21.5	20.1	16.5	13.8	0.94	0.91

We have experimentally tested the beam shaping performance of the functional facet by observing the first diffraction order of the far field image for two types of accelerating beams, Airy and Parabolic beams. These beams propagate in a parabolic trajectory ("accelerating" in the transverse plane to the propagation direction) without changing their shape over a finite distance [9,10]. Fig. 3 presents a comparison between theoretical beam shapes (upper row) and measured beams in the first diffraction order of both frequencies. High spatial correlation, ≥90%, between measured and theoretical beams is obtained, as summarized in Table 1. We measured the accelerating features of the beams and verified that all three beams, in both frequencies, exhibit the expected parabolic acceleration curves.

We also characterized the generated vortex beams, Fig. 4 summarizes the results. Part (a) in the figure shows an image of the mask on the facet as recorded after a 4f lens system. Part (b) shows the theoretical beams and Parts (c) and (d) are measured beam shapes for both frequencies. The spatial correlation of the beams and shaping efficiencies are presented in Table 1. As an additional check, we evaluated the M^2 of the generated beams. For the topological charge of $+1$ the values are 2.21 ± 0.15 and 2.09 ± 0.1 for FF and SH, respectively, whereas the theoretical value is 2 [16]. For the topological charge of $+2$ the values are 3.36 ± 0.14 and 3.23 ± 0.12 for FF and SH, respectively, the theoretical value is 3 [16]. The radius of the beam is expected to be proportional to $\sqrt{l_c\lambda}$ [11], where l_c is the topological charge and λ is the wavelength. We verified that the above relation exists in the measured beams. The measured total external nonlinear conversion efficiency in the KTP crystal, for peak power, for a structure generating a beam with a topological charge of $+1$ was 4.2×10^{-3} [%W^{-1}]. For reference, the conversion efficiency without the gold layer was 3.3×10^{-2} [%W^{-1}].

An additional functionality that was checked is focusing of the generated beam. A quadratic phase modulation was applied to the binary transmission hologram [12],

$$t(y,z)=0.5\left[1+sign\left\{\cos\left(2\pi y f_{carrier}+\frac{k(y^2+z^2)}{2f}\right)\right\}\right] \quad (3)$$

where k is the SH wave-vector and f is the desired focal length. Focusing at a distance of 6 cm (3 cm) was observed at the first diffraction order for the SH (FF) beams. The different focal length of the SH and FF beams, owing to the different wave-vectors, provides another way to separate the beams in addition to their angular separation. Comparison between SH measured and simulated results for this case are presented in Fig. 5, parts (a) and (b). Numerical simulations were performed based on the split-step Fourier method [17], where the interacting beams are propagated in 0.1 μm increments and the linear and nonlinear parts of the wave equation are solved separately.

Note that the beam at the −1 order (on the left to the zero order) is diverging, since we have a negative lens for this order. 20.3% of the SH power was predicted to be in the focusing diffraction order, the measured fraction was only 10.5%, we will suggest an explanation to this difference in the discussion section. A lens can also be implemented in an amplitude mask without encoding a carrier frequency, in this case the pattern forms the well known rings of Fresnel zone plates.

Moving now to the spatial filtering experiment, the quality of the beam was evaluated in terms of its M^2, which for a diverging beam can be calculated using the relation $W_y^2(x)=W^2{}_{0y}+(M_y^2)^2((X-X_0)/X_R)^2$, where W_y is twice the standard deviation (σ_y), which is calculated from the second moment of the transverse distribution; X_0 and W_{0y} are the waist location and size, respectively, and X_R is the Rayleigh length. The transverse profiles were measured with a laser beam profiler at the waist and a few Rayleigh lengths away, $2\sigma_y$ values were estimated calculating the second moment of the measured profiles. The evaluated M^2 of the original Gaussian FF beam is 1.21 ± 0.012. We deliberately deteriorated the quality of this beam by partially blocking it and the new evaluated M^2 was 2.96 ± 0.1. This beam entered the nonlinear crystal and both it and its' SH were filtered by a patterned pinhole with a radius of 130 μm at the crystal's output facet, M^2 was evaluated for both beams. The result for FF was 1.32 ± 0.1 and for SH 1.18 ± 0.013, meaning that both beams were of higher quality in comparison with the original unfiltered pumping beam. Fig. 6 part (a), shows (in normalized units) the measured beam radius as a function of the distance from the beams' waist for the above mentioned case. We also simulated a case in which a Gaussian pump beam was deteriorated by blocking the center of the beam.

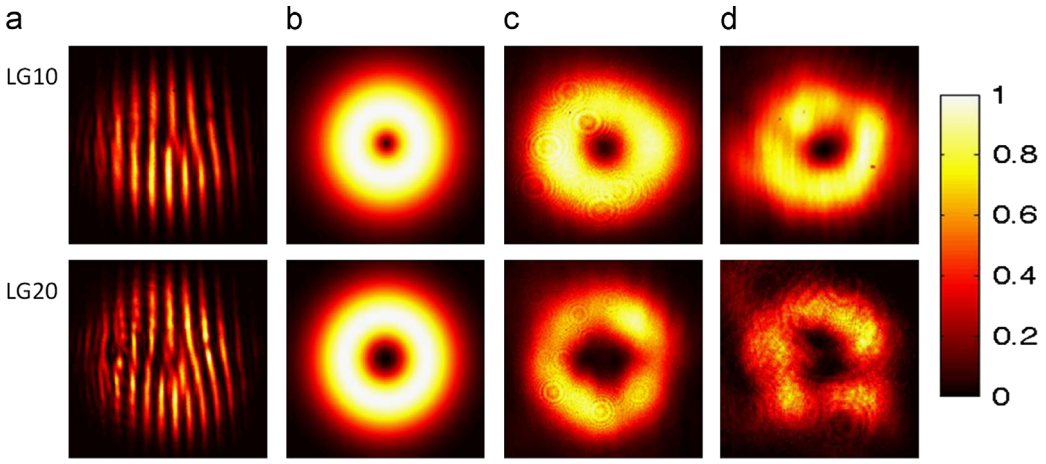

Fig. 4. Vortex beams with topological charge of $+1$ (top row) and $+2$ (bottom row). Image of the facet with a 4f lens system, showing the pattern that generates a vortex beam (a), theoretical beam (b), FF generated beam (c), and SH generated beam (d).

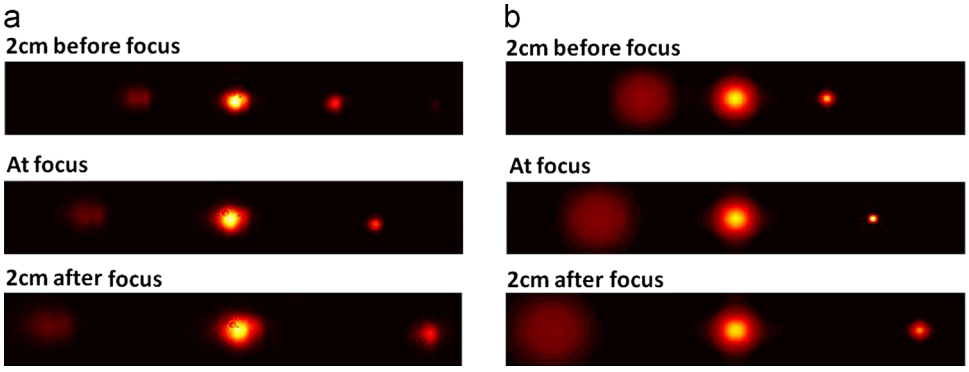

Fig. 5. Focusing—SH diffraction pattern before, at and after focus, measured (a) and simulated (b).

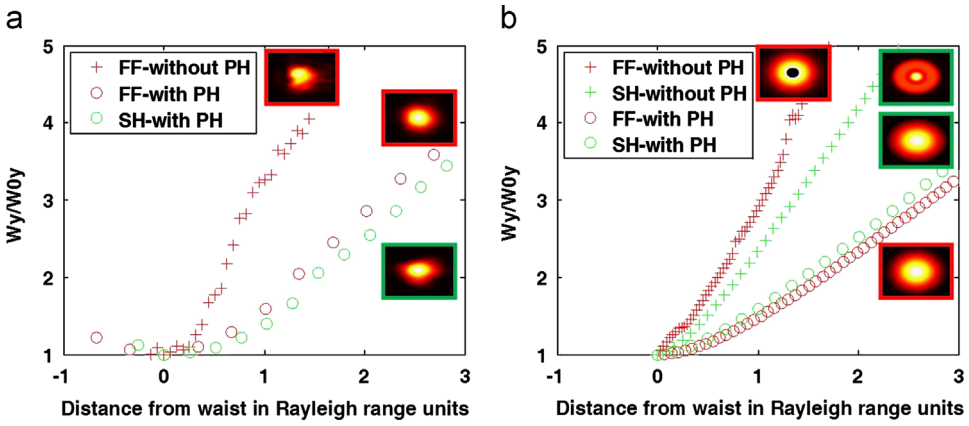

Fig. 6. Spatial filtering—normalized beam radius vs. the normalized distance from the beams' waist, measured (a) and simulated (b). Beam shapes for the different cases are shown in the insets. PH – Pinhole.

We blocked a radius of 32 μm in a 100 μm waist beam and the results are shown in Fig. 6 part (b). The evaluated M^2 for the pump in this case was 3.07 ± 0.1. It is important to note that the doubling process itself provides a certain amount of beam clean-up, even without a pinhole. Indeed, a smaller M^2 of 2.01 ± 0.03 was calculated for the generated SH beam, but it can be further improved by spatial filtering with the pinhole. The FF and SH that passed through a patterned pinhole with a radius of 130 μm were high quality beams, with M^2 of 1.03 ± 0.001 for the FF and M^2 of 1.09 ± 0.002 for the SH beam. 9% of the SH and 15% of the FF power were lost due to passing through the pinhole.

3. Discussion

The total FF transmittance of the structures was consistently higher than predicted. In addition, the shaping efficiency, i.e. the percentage of the diffracted light in the first diffraction order, was lower than predicted for both FF and SH beams (Table 1 and previously mentioned result for the lens structure). Both observations lead to the conclusion that the modulation in the structures was not 0–1 as expected. Instead, a fraction of the power must have passed through the regions where the gold was not removed. The thickness of the gold in our samples was 80 nm, according to

absorption calculations this thickness is not supposed to pass any light at 1064.5 nm. We assume that the observed transmission might be due to inhomogeneity of the sputtered layer. The transmission of the gold can be quantified by comparing the experimental and predicated diffraction efficiencies. For example, for the Airy beam case, for a perfect 0–1 modulation the expected percentage of power at the first diffraction order for FF is 23.1%, if however, the modulation is 0.12–1 the expected percentage is only 8.7%. From this we can estimate that the transmission in the metal coated regions was approximatly12%.

Two-dimensional beam shaping in nonlinear crystals was previously reported in Refs. [6,7], in both cases the required poling pattern of the nonlinear crystal is two-dimensional, thus complicating the fabrication process of the crystal and limiting the choice of crystals. In addition, the resulting conversion efficiency is very low since the vectorial condition of phase-matching the nonlinear process is not completely fulfilled. Conversion efficiency reported here, when taking into account the difference in crystal lengths, is about 5 orders of magnitude larger than previously reported numbers.

Beam shaping as described here was achieved with an amplitude mask, the disadvantage of this is the loss of SH power, approximately 50%, generated in the crystal when passing through the facet. However, by using a transparent and conductive material at the crystal facet, for example indium tin oxide (ITO) instead of gold, we can realize phase masks. The mask can be patterned according to Ref. [12], where the binary modulation would be between 0 and π phase added to the SH beam passing through the ITO. The advantage of phase masks compared to amplitude masks is in the total efficiency of the diffraction pattern and the diffraction efficiency. In phase masks, FF would also be shaped, but usually with a much smaller diffraction efficiency. As with amplitude masks, the shaped frequencies would be spatially separated.

4. Conclusion

In this work we have presented and experimentally verified a new method of adding functionality to a nonlinear process. This is achieved by sputtering a gold layer on top of the exit facet of a nonlinear crystal and patterning the layer with FIB. The result is a device that can be designed to shape and manipulate the beams in the nonlinear interaction without compromising the efficiency of the interaction. We have shown here three functions—two-dimensional beam shaping, focusing and spatial filtering, but other optical functions (e.g. beam splitting) can be realized in a similar manner. For the first two cases, the FF and SH beams are obtained at different angles (and different focal lengths in the case of a lens), hence can be easily separated. Furthermore, whereas here we demonstrated this method on a bulk nonlinear device, the high resolution of the FIB milling process enables to apply this method at the exit facets of nonlinear waveguides as well.

Acknowledgments

This work was supported by the Israel Science Foundation, Grant no. 774/09 and The Israeli Ministry of Science.

References

[1] J.R. Kurz, A.M. Schober, D.S. Hum, A.J. Saltzman, M. Fejer, IEEE Journal of Selected Topics in Quantum Electronics 8 (2002) 660.
[2] Y. Qin, C. Zhang, Y. Zhu, X. Hu, G. Zhao, Physical Review Letters 100 (2008) 063902.
[3] T. Ellenbogen, A. Ganany, A. Arie, Optics Express 16 (2008) 3077.
[4] T. Ellenbogen, N. Voloch-Bloch, A. Gannay-Padowicz, A. Arie, Nature Photonics 3 (2009) 395.
[5] A. Shapira, I. Juwiler, A. Arie, Optics Letters 36 (2011) 3015.
[6] A. Shapira, R. Shiloh, I. Juwiler, A. Arie, Optics Letters 37 (2012) 2136.
[7] N. Voloch-Bloch, K. Shemer, A. Shapira, R. Shiloh, I. Juwiler, A. Arie, Physics Review Letters 108 (2012) 233902.
[8] B.R. Brown, A.W. Lohmann, Applied Optics 5 (1996) 967.
[9] G.A. Siviloglou, J. Broky, A. Dogariu, D.N. Christodoulides, Physics Review Letters 99 (2007) 213901.
[10] M.A. Bandres, Optics Letters 33 (2008) 1678.
[11] L. Allen, M.W. Beijersbergen, R.J.C. Spreeuw, J.P. Woerdman, Physical Review A 45 (1992) 8185.
[12] W.H. Lee, Applied Optics 18 (1979) 3661.
[13] I. Dolev, A. Ganany-Padowicz, O. Gayer, A. Arie, J. Mangin, G. Gadret, Applied Physics B 96 (2009) 423.
[14] M. Yamada, N. Nada, M. Saitoh, K. Watanabe, Applied Physics Letters 62 (1993) 435.
[15] K. Kato, E. Takaoka, Applied Optics 41 (2002) 5040.
[16] S. Saghafi, C.J.R. Sheppard, Optics Communications 153 (1998) 207.
[17] G.P. Agrawal, Nonlinear Fiber Optics, Academic, Boston, Mass., 1995.